Optics Letters

Signal-to-noise ratio improvement of photonic time-stretch coherent radar enabling high-sensitivity ultrabroad W-band operation

Na Qian, Weiwen Zou,* Siteng Zhang, and Jianping Chen

State Key Laboratory of Advanced Optical Communication Systems and Networks, Department of Electronic Engineering, Shanghai Jiao Tong University, Shanghai 200240, China
Corresponding author: wzou@sjtu.edu.cn

The signal-to-noise ratio (SNR) of the photonic time-stretching receiver in the photonic time-stretch coherent radar (PTS-CR) system is theoretically analyzed. According to the analysis based on the erbium-doped fiber amplifier (EDFA) characteristic, it is found that the SNR is dominantly determined by the input optical power of the EDFA. With the improvement of the SNR of the photonic time-stretching receiver, the radar detection sensitivity is consequently enhanced. Furthermore, a PTS-CR system operating at W band with the ultrabroad bandwidth of 12 GHz is experimentally enabled, leading to the range resolution of ~1.48 cm in dual-target detection. © 2018 Optical Society of America

https://doi.org/10.1364/OL.43.005869

With the advantage of high resolution, antijamming, and a narrow beam, millimeter-wave radar provides access to applications such as accuracy ranging, precision imaging, and foreign body detection [1,2]. The signal transmitted by the millimeter-wave radar has the characteristics of high-frequency band and broad bandwidth [3,4]. However, suffering severely from the issues of timing jitter and noise, the traditional analog to digital conversion (ADC) technology is not reliable to deal with the ultrabroad millimeter-wave radar signal [5,6]. Thanks to the development of ADC based on photonic time-stretch [7,8], bandwidth is compressed before sampling and thus a broad bandwidth radar signal can be captured and processed. Recently, an X-band photonic time-stretch coherent radar (PTS-CR) employing a time-stretching process in the receiver was experimentally demonstrated [9,10].

The W-band signal exceeds the working bandwidth of the general electro-optical modulators. Traditional electrical down-conversion is needed before the electro-optical modulation [1], bringing non-negligible attenuation to the signal. Besides, the radar echo signal is acyclic and difficult to rebuild so that maintaining the quality of the echo signal is crucial in the receiver. Therefore, the radar receiver with high signal-to-noise ratio (SNR) is desired for high sensitivity. Although photonic

time-stretch can break the bandwidth limit of the millimeter-wave radar receiver, the stretched signal is seriously distorted by noise, especially the amplified spontaneous emission beat noise introduced by an optical amplifier [11]. To compensate the power loss caused by a long dispersion compensation fiber (DCF), an optical amplifier is needed in a common time-stretch link [12], whose performance directly affects the quality of the received signal [13]. Distributed optical amplification in the dispersive fiber has been demonstrated in the time-stretch spectroscopy to maintain the appropriate signal level [6,14], whereas it is limited by the gain and the pump efficiency. To date, discrete optical amplifiers such as an erbium-doped fiber amplifier (EDFA) with a higher gain have been employed in the photonic time-stretching receiver of the PTS-CR [9,10]. However, the noise feature of discrete optical amplifiers should have a strong impact on the sensitivity and range resolution of the PTS-CR.

In this Letter, we investigate the SNR of the photonic time-stretching receiver of the PTS-CR based on discrete optical amplifiers. The analysis based on the characteristic of the EDFA reveals that a higher SNR can be obtained by adjusting the input optical power of the EDFA. Thus, the sensitivity of the radar is enhanced. It is experimentally verified that the SNR of the photonic time-stretching receiver can be improved by optimizing the input optical power of the EDFA. A PTS-CR operating at W band with the measured range resolution of ~1.48 cm is experimentally demonstrated when the SNR of the photonic time-stretching receiver is improved.

Figure 1 illustrates the experimental setup of the PTS-CR operating at W band under the assistance of a W-band frontend. (See the Fig. 1 caption for the definition of the acronyms used in both this figure and in the text below.) The PTS-CR consists of two parts: the photonic transmitter and the photonic time-stretching receiver. The W-band frontend enables the PTS-CR to operate at W band. Optical pulse trains generated by a passively mode-locked laser (PMLL, Menlo Systems, C-Fiber) with the repetition rate of 100 MHz are equally divided by OC1. The optical pulses divided for W-band signal generation are dispersed by the dispersion element (DE1) with
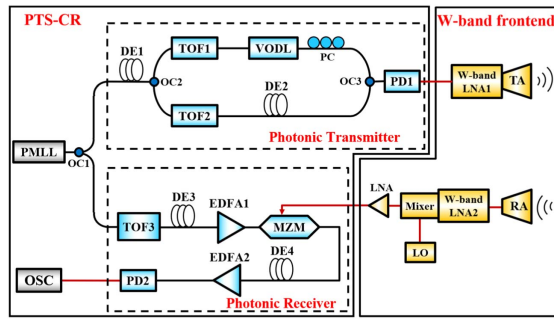
Fig. 1. Experimental setup of the PTS-CR under assistance of a W-band frontend. PMLL, passively mode-locked laser; OC, optical coupler; DE, dispersion element; TOF, tunable optical filter; VODL, variable optical delay line; PC, polarization controller; PD, photodetector; EDFA, erbium-doped fiber amplifier; MZM, Mach–Zehnder modulator; LNA, low noise amplifier; LO, local oscillator; TA, transmitting antenna; RA: receiving antenna; OSC, oscilloscope.

Fig. 2. (a) Detailed setup of the photonic time-stretching receiver and (b) schematic of a modulated optical pulse passing through EDFA2. DE4 consists of three fiber segments of DE4-1, DE4-2, and DE4-3, and EDFA2 is inserted at A, B, C, and D, respectively.

a relatively large dispersion value. They are split by OC2 and filtered separately by TOF1 (Alnair Labs, CVF-300CL) and TOF2 (Alnair Labs, CVF-220CL). The carrier frequency of the signal is determined by the difference between the central wavelengths of the TOFs [15]. DE2 introduces extra dispersion to the optical pulses in the lower arm, determining the sweep bandwidth of the generated signal. In the upper arm, a VODL (General Photonics, MDL-002) is used to make the pulses in two arms aligned, and a polarization controller (PC) is added to optimize the interference intensity. After coupled by OC3, the optical signal is converted to the linear frequency modulation (LFM) pulse by PD1 (Finisar, XPDV4121R). Before being transmitted by the antenna (TA), the generated LFM signal is amplified by a W-band low noise amplifier (LNA1, Milltech, LNA-10-02590). The W-band LNA2 (Milltech, LNA-10-02590), W-band mixer (SAGE, SFB-10-N1), and LO (SAGE, SOM-10405213-10-S1) in the W-band frontend are used to amplify and down-convert the received echo signal. Another LNA (Photline, DR-AN-20-HO) is added to compensate the loss introduced by down-conversion. In the photonic time-stretching receiver, the reception aperture depends on the bandwidth of TOF3 and dispersion value of DE3. The down-converted echo is modulated onto the prechirped pulse via MZM (Photline, MXAN-LN-20). The modulated pulse is amplified by EDFA2 (Calmar, Coronado) and stretched by DE4. After the photonic time-stretching process, the optical pulse is transferred to the electric pulse by PD2 (bandwidth, 18 GHz) and digitized by an oscilloscope (Keysight MSO804A). Note that attention has been paid to ensure the input optical power of the PD is below the saturation power of the PD.

The detailed setup of the photonic time-stretching receiver in Fig. 1 is separately depicted in Fig. 2(a). Two EDFAs are employed in this link. EDFA1 is added to compensate the optical losses caused by DE3 and TOF3 in case of the unsatisfactory modulation efficiency caused by low optical power to the MZM [11]. EDFA2 is employed to amplify the modulated optical pulses. Figure 2(b) depicts the schematic of a modulated optical pulse passing through EDFA2 with different input optical pulse power. According to the gain curve of the EDFA, when input optical pulse power is relatively low the gain of the signal modulated on the pulse is linear. However, as the
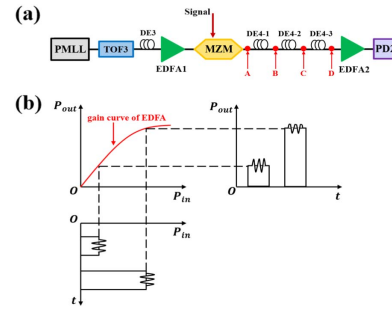
input optical pulse power increases, the amplifier tends to saturate. As a result, the signal modulated on the pulse will be distorted. The gain G of the modulated microwave signal can be expressed as

$$G(P) = \frac{G_0}{1 + (\omega - \omega_0)^2 T^2 + \frac{P}{P_{\text{sat}}}}, \tag{1}$$

where G_0 is the linear gain, P_{sat} is the optical saturation power, and ω_0 is the central frequency of EDFA2. P is the input optical pulse power, ω is the frequency of the input optical pulse, and T is the relaxation time. According to the analysis in [11], the SNR of the photonic time-stretching receiver is mainly limited by the ASE noise. The SNR at the output of the photonic time-stretching receiver of the PTS-CR is derived according to [16], which is described by

$$\text{SNR}_{\text{out}} = \frac{P_{\text{out}}}{N_{\text{out}}} = \frac{m^2 P_{\text{sig}} L_4 G_2 R_{PD}}{M^2 R_{PD} B_e (\rho_{\text{ASE}}^1 L_m L_4 G_2 + \rho_{\text{ASE}}^2)}$$
$$= \frac{m^2 P_{\text{sig}}}{M^2 B_e \left(\rho_{\text{ASE}}^1 L_m + \frac{\rho_{\text{ASE}}^2}{L_4 G_2} \right)}, \tag{2}$$

where P_{out} is the power of the time-stretched signal after optical-electronic conversion, and N_{out} is the power of the ASE noise at the output. m is the modulation index, P_{sig} is the power of the microwave signal, and M is the stretch factor. L_m and L_4 correspond to the loss of the MZM and DE4, G_2 is the gain of EDFA2, which is subjected to the input optical pulse power, and B_e is the electric bandwidth. Furthermore, ρ_{ASE}^1 and ρ_{ASE}^2 are the ASE power spectral densities of EDFA1 and EDFA2, which are also related to each amplifier's gain as

$$\rho_{\text{ASE}}^i = 2n_{sp}(G_i - 1)h\nu, \tag{3}$$

where $i = 1$ or 2 corresponds to EDFA1 or EDFA2, h is Planck's constant, and ν is the optical frequency. n_{sp} is the population inversion parameter depending on the pump conversion efficiency [17], which relates to the input optical power of EDFA. Under the linear gain condition, the conversion efficiency is high. If the input power is close to or larger than the saturation power, the efficiency becomes lower. According to Eqs. (1)–(3), the noise performance of EDFA2 and the SNR$_{\text{out}}$ of a photonic time-stretching receiver with specific dispersion elements are intrinsically determined by the input optical pulse power to EDFA2.
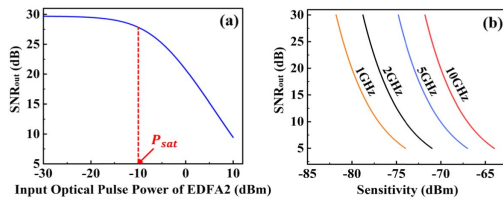
Fig. 3. (a) Simulation of the SNR_{out} of the photonic time-stretching receiver as a function of the input optical pulse power of EDFA2. (b) Analysis of the relation between the SNR_{out} and the sensitivity of the PTS-CR with different bandwidths.

Fig. 4. Experiment results of the SNR_{out} with different input optical pulse powers of EDFA2.

To quantitatively analyze the relation between SNR_{out} and input optical pulse power of EDFA2, a numerical simulation is implemented and the result is demonstrated in Fig. 3(a). The linear gain G_0 of EDFA2 is set to be 30 dB and the optical saturation power P_{sat} is −10 dBm. The modulation index is $m = 0.3$ and the stretch factor is $M = 4$. The loss of the MZM is 7 dB. The power of the microwave signal is set to be 10 dBm. When the input optical pulse power is much less than the P_{sat}, the SNR_{out} is maintained at the optimal value. With the increase of the input power, the SNR_{out} becomes lower, and when the input power is larger than P_{sat}, the SNR_{out} starts to decline rapidly. The simulation result shows that the optimal SNR_{out} of the photonic time-stretching receiver can be obtained when the input optical power of EDFA2 is ensured to be much smaller than the P_{sat}.

Furthermore, in radar systems the receiver sensitivity is usually given by [18]

$$S_{i\,min} = KT_0 B_e F, \qquad (4)$$

where $S_{i\,min}$ is the sensitivity, KT_0 is the input thermal noise floor per unit bandwidth, and F is the noise figure of the receiver. According to the definition of the noise figure [19], the sensitivity of the photonic time-stretching receiver in the PTS-CR can be expressed as

$$S_{i\,min} = KT_0 B_e \frac{SNR_{in}}{SNR_{out}}. \qquad (5)$$

The numerical simulation based on Eq. (5) is additionally implemented to intuitively identify the relation between the SNR_{out} and sensitivity of the PTS-CR. The sensitivity as a function of the SNR_{out} of the photonic time-stretching receiver, under different bandwidths ($B_e = 1$ GHz, 2 GHz, 5 GHz, or 10 GHz) of the receiver, is depicted in Fig. 3(b). It is indicated that the higher SNR_{out} leads to a lower minimum detectable signal power of the radar, meaning a better sensitivity. It shows that with a broader bandwidth, the higher SNR_{out} of the photonic time-stretching receiver is required for the same sensitivity. According to the above analysis and simulation, the ultrabroad bandwidth PTS-CR operating at W band with high sensitivity calls for a high SNR. A high SNR photonic time-stretching receiver corresponds to the low input optical pulse power of EDFA2 in Fig. 3(a). Therefore, an ultrabroad bandwidth PTS-CR with high SNR and high sensitivity can be achieved by controlling the input optical power of EDFA2 in the photonic time-stretching receiver according to Fig. 3(a).

The relation between the SNR_{out} of the photonic time-stretching receiver and the input optical pulse power of EDFA2 is experimentally carried out based on Fig. 2(a). It is
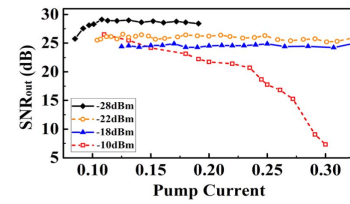
noted that DE4 consists of three fiber segments introducing different optical losses. By placing EDFA2 at different locations of A, B, C, and D among these segments [see Fig. 2(a)], the input optical pulse power of EDFA2 is −10 dBm, −18 dBm, −22 dBm, and −28 dBm, respectively. The frequency of signal to be processed is 4 GHz generated by a microwave synthesizer (Keysight, N5183B). Figure 4 illustrates the experimental results. Three sets of data with the input power lower than the optical saturation power of EDFA2 (−10 dBm) show that the SNR_{out} is relatively close. However, another set where the input power is the saturation power shows a lower SNR_{out}. The comparison of the SNR_{out} value verifies the numerical analysis [see Fig. 3(a)]. It is also found that the SNR_{out} is maintained at a quite stable value as the pump current increases in these three sets of data (−28 dBm, −22 dBm, and −18 dBm). Meanwhile, the SNR_{out} declines along with the growth of the pump current in another set of data. It reveals that a quite lower pump conversion efficiency causes the noise deterioration as the pump current increases. So, the SNR_{out} declines further. The experimental results verify that the SNR_{out} of the photonic time-stretching receiver can be observably improved when the optical pulse power into EDFA2 is set dramatically less than the saturation power.

After the SNR and sensitivity of the photonic time-stretching receiver are improved, the PTS-CR enabling ultrabroad W-band operation is experimentally demonstrated based on the experimental setup depicted in Fig. 1. In the photonic transmitter, the center wavelength offset between TOF1 and TOF2 is 0.74 nm corresponding to the 92.5 GHz center frequency, while these TOFs are set to have the same bandwidth of 2.22 nm. The dispersion value of DE1 is −880.3 ps/nm and the value of DE2 is −40 ps/nm. Referring to [15], the generated W-band signal has a nominal bandwidth of ∼12 GHz, which is amplified by a W-band LNA and transmitted by an antenna (Tx). Another antenna acting as the receiving antenna (Rx) is placed side by side to the Tx antenna. The echo signal collected by the Rx antenna is amplified and down-converted. In the photonic receiver, the bandwidth of TOF3 is 2.5 nm and the dispersion value of DE3 is −986.5 ps/nm; this determines the reception aperture of ∼2.5 ns. The dispersion value of DE4 is −2987 ps/nm and the stretch factor is 4. Two targets, A and B (2-mm-thin metal flats with the sizes of 15 cm × 10 cm), with a ∼5 cm distance apart are positioned ∼1.35 m away from the antennas, schematically depicted in Fig. 5(a). Figure 5(b) shows the down-converted and stretched reference signal observed from the oscilloscope. Its bandwidth is ∼3 GHz as depicted in the short-time Fourier transform analysis in Fig. 5(b). As depicted in the insert of Fig. 5(b), the autocorrelation result with a 5.21 cm width also verifies the bandwidth of ∼3 GHz. Since the stretch factor
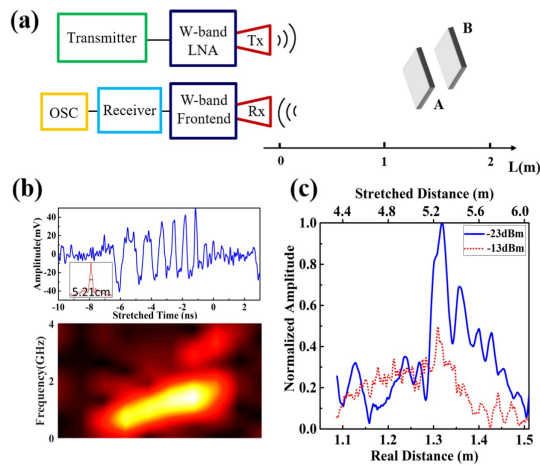
Fig. 5. Comparison of the photonic time-stretching receiver with and without SNR improvement in the PTS-CR system at W band. (a) Schematic of dual-target detection. (b) Detected reference signal after down-conversion and time-stretching in the time domain (top), the frequency domain (down), and its autocorrelation (insert). (c) Pulse compression results of the photonic time-stretching receiver (solid line) with and (dashed line) without SNR improvement.
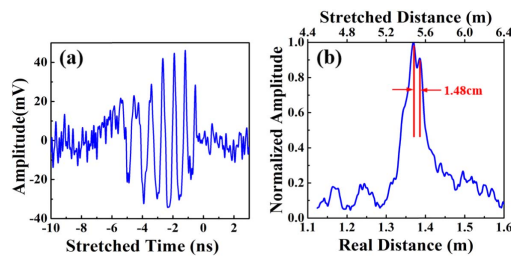
Fig. 6. Measurement results of the dual-target detection with the improved SNR of the photonic time-stretching receiver. (a) The echo signal after down-conversion and time-stretching. (b) The result after the pulse compression processing.

is 4, the original bandwidth of the generated W-band signal is $B_e = \sim 12$ GHz, which agrees with the nominal value.

The detection results of the photonic time-stretching receiver are shown in Fig. 5(c). According to Fig. 3(a), when the input optical pulse power of EDFA2 is −23 dBm, the SNR is relatively higher than the situation when the input optical pulse power is −13 dBm. Owing to the higher SNR of the photonic time-stretching receiver, it can be found that there are two peaks at ∼1.32 m and ∼1.37 m corresponding to the targets A and B in Fig. 5(c). However, there is only one peak when the SNR is low.

The nominal range resolution is estimated to be 1.25 cm according to $\delta_r = \frac{C}{2B_e}$, where C is the velocity of the light. The range resolution of the PTS-CR operating at W band is also experimentally demonstrated. The setup is the same as Fig. 5(a), except that two targets are closely placed side by side with ∼1.5 cm distance apart. The echo signal of targets A and B passing through the W-band frontend and photonic time-stretching receiver is illustrated in Fig. 6(a). After the pulse compression algorithm [9], the result is plotted in Fig. 6(b)

against the time-stretched distance (top horizontal axis) and the real distance before the time-stretching processing (bottom horizontal axis). As depicted in Fig. 6(b), two targets separated by 1.48 cm are distinguishable after the pulse compression process, verifying the nominal range resolution of $\delta_r = 1.25$ cm.

In conclusion, we have analyzed and improved the SNR of the PTS-CR's photonic time-stretching receiver. Based on the analysis, the SNR is influenced by the input optical power of the EDFA employed in the photonic time-stretching receiver. Experiments have been carried out by controlling different input optical power of the EDFA to verify the analysis. The SNR of the photonic time-stretching receiver was improved, and thus the receiving sensitivity was experimentally enhanced in the ultrabroad PTS-CR. Consequently, the range resolution of the PTS-CR system operating at W band with the bandwidth of 12 GHz was tested to be ∼1.48 cm. The influence of the W-band frontend (including W-band mixer, LO, and LNAs) to the performance of the PTS-CR operating at W band is now under investigation. Subsequent detection experiments will be performed in a microwave darkroom to avoid clutter interference.

REFERENCES

1. Y. Li, A. Rashidinejad, J. M. Wun, D. E. Leaird, J. W. Shi, and A. M. Weiner, Optica **1**, 446 (2014).
2. T. F. Tseng, J. M. Wun, W. Chen, S. W. Peng, J. W. Shi, and C. K. Sun, Opt. Express **21**, 14109 (2013).
3. S. Xu, W. Zou, G. Yang, and J. Chen, Chin. Opt. Lett. **16**, 062801 (2018).
4. F. Zhang, Q. Guo, Z. Wang, P. Zhou, G. Zhang, J. Sun, and S. Pan, Opt. Express **25**, 16274 (2017).
5. P. Ghelfi, F. Laghezza, F. Scotti, G. Serafino, A. Capria, S. Pinna, D. Onori, C. Porzi, M. Scaffardi, A. Malacarne, V. Vercesi, E. Lazzeri, and A. Bogoni, Nature **507**, 341 (2014).
6. A. Khilo, S. J. Spector, M. E. Grein, A. H. Nejadmalayeri, C. W. Holzwarth, M. Y. Sander, M. S. Dahlem, M. Y. Peng, M. W. Geis, N. A. DiLello, J. U. Yoon, A. Motamedi, J. S. Orcutt, J. P. Wang, C. M. Sorace-Agaskar, M. A. Popović, J. Sun, G. Zhou, H. Byun, J. Chen, J. L. Hoyt, H. I. Smith, R. J. Ram, M. Perrott, T. M. Lyszczarz, E. P. Ippen, and F. X. Kärtner, Opt. Express **20**, 4454 (2012).
7. A. Mahjoubfar, D. V. Churkin, S. Barland, N. Broderick, S. K. Turitsyn, and B. Jalali, Nat. Photonics **11**, 341 (2017).
8. F. Coppinger, A. S. Bhushan, and B. Jalali, IEEE Trans. Microw. Theory Tech. **47**, 1309 (1999).
9. W. Zou, H. Zhang, X. Long, S. Zhang, Y. Cui, and J. Chen, Sci. Rep. **6**, 19786 (2016).
10. S. Zhang, W. Zou, N. Qian, and J. Chen, IEEE Photon. Technol. Lett. **30**, 1028 (2018).
11. Y. Han and B. Jalali, J. Lightwave Technol. **21**, 3085 (2003).
12. J. Zhang and J. Yao, Optica **1**, 64 (2014).
13. M. Shiraiwa, A. Kanno, T. Kuri, P. T. Dat, Y. Awaji, N. Wada, and T. Kawanishi, *International Topical Meeting on Microwave Photonics and the 9th Asia-Pacific Microwave Photonics Conference* (2014), p. 21.
14. K. Goda and B. Jalali, Nat. Photonics **7**, 102 (2013).
15. H. Zhang, W. Zou, and J. Chen, Opt. Lett. **40**, 1085 (2015).
16. A. S. Bhushan, P. V. Kelkar, B. Jalali, O. Boyraz, and M. Islam, IEEE Photon. Technol. Lett. **14**, 684 (2002).
17. C. R. Giles and E. Desurvire, J. Lightwave Technol **9**, 271 (1991).
18. M. I. Skolnik, *Radar Handbook* (1970).
19. H. T. Friis, Proc. IRE **32**, 419 (1944).